Environ Earth Sci (2016) 75:1119
DOI 10.1007/s12665-016-5910-0

ORIGINAL ARTICLE

Chemical and strontium isotopic characteristics of the rivers around the Badain Jaran Desert, northwest China: implication of river solute origin and chemical weathering

Wenjing Liu[1,2,3] · Hao Jiang[1,3] · Chao Shi[1,3] · Tong Zhao[1,3] · Chongshan Liang[4] · Jian Hu[4] · Zhifang Xu[1,3]

Received: 10 March 2016 / Accepted: 18 July 2016 / Published online: 26 July 2016

Abstract The chemical and strontium isotopic compositions of four major rivers (Heihe, Shule, Beida, and Shiyang) around the Badain Jaran Desert, northwestern China, were measured to understand the solute sources of surface water and rock weathering in the arid region. These rivers have high total cationic charge (TZ^+) and total dissolved solids (TDS), averaging at 7379 μEq and 511 mg l^{-1}, which are significantly higher than the global river average. The increase in TDS and major ions (Na^+, Cl^-, and SO_4^{2-}) and TDS concentrations from upper to lower reaches is ascribed to the evaporite dissolution and the effect of evaporation in the arid and semiarid areas. $^{87}Sr/^{86}Sr$ isotopic ratios of these rivers range between 0.71019 and 0.71628, with an average of 0.71328. The chemical and $^{87}Sr/^{86}Sr$ isotopic analyses indicate that three reservoirs (evaporites, carbonates, and silicates) contribute to the total dissolved loads. The contributions of the different reservoirs to the dissolved load are first calculated using a forward method in this area. The calculated results show that the dissolved cation load is dominated by carbonates weathering and evaporites dissolution, and their contribution account for about 80 % of the total dissolved cations for the rivers around the Badain Jaran Desert. The proportion of the dissolved cations from silicates weathering is 23.5, 10.8, 12.1, and 18.2 %, and the weathering rate of silicates is 0.81, 0.76, 2.04, and 0.93 ton km^{-2} a^{-1} for Heihe, Shule, Beida, and Shiyang, respectively.

Keywords Badain Jaran Desert · Northwestern China · River water · Strontium isotope · Rock weathering

✉ Zhifang Xu
zfxu@mail.iggcas.ac.cn

[1] Key Laboratory of Shale Gas and Geoengineering, Institute of Geology and Geophysics, Chinese Academy of Sciences, Beijing 100029, China

[2] Earth and Environmental Systems Institute and the Department of Geosciences, The Pennsylvania State University, University Park, PA 16802, USA

[3] University of Chinese Academy of Sciences, Beijing 100049, China

[4] State Key Laboratory of Environmental Geochemistry, Institute of Geochemistry, Chinese Academy of Sciences, Guiyang 550002, Guizhou, China

Introduction

The hydro-geochemical investigation of river waters provides important information on chemical and isotopic compositions of the upper continental crust, weathering rates of rock/soil, and the major ion geochemical cycles at basin and global scales (Stallard and Edmond 1983, 1987; Sarin et al. 1989; Palmer and Edmond 1992; Zhang et al. 1995a; Huh et al. 1998; Gaillardet et al. 1997; Viers et al. 2000; Qin et al. 2005; Xu and Liu 2010; Jin et al. 2011). Since the pioneering work of Gibbs (1970), many studies have focused on river geochemistry, including small watershed for effect of lithology and climate control on rock weathering (e.g., Bluth and Kump 1994; White and Blum 1995; Gislason et al. 1996; Louvat and Allégre 1997), and the world's major rivers for a more global perspective (e.g., Hu et al. 1982; Berner et al. 1983; Meybeck 1987; Summerfield and Hulton 1994; Gaillardet et al. 1999; Galy and France-Lanord 1999; Chen et al. 2002; Chetelat et al. 2008). Up to now, the studies on geochemistry of rivers draining desert areas are still scarce. These rivers are generally not included in previous studies on chemical weathering at the global scale due to their small discharge.

Researches about geochemistry of rivers in China are mainly focused on large rivers in eastern monsoon region, such as the Changjiang River and Yellow River (Zhang et al. 1995a; Chen et al. 2002; Wu et al. 2005, 2008; Chetelat et al. 2008; Xu et al. 2011), and Pearl River (Zhang et al. 2007a; Gao et al. 2009; Xu and Liu 2007, 2010). However, inland rivers under arid and semi-arid climate in northwest China are not arousing enough attention. Four major rivers (Heihe, Shule, Beida and Shiyang) around the Badain Jaran Desert in northwest China are investigated in this study. This paper presents the chemical and strontium isotopic compositions for these rivers in the arid and semiarid environment. The purpose of this paper is to discuss the hydro-chemical processes controlling the water geochemistry, decipher the different sources of solutes, and to quantify the contributions of the various sources to the dissolved loads. The results can provide information on the chemical weathering and the controls over water chemistry of the river waters in the arid environments.

Natural setting of study area

The study area is located in northwestern China, and it is bordered by the Tengger Desert on the east, the Badain Jaran Desert on the northeast, and the Qilian Mountains on the southwest (Fig. 1). According to geographical characteristics, the study area can be divided into the southern Qilian Mountains and northern plains region. The elevation in the plains ranges between 920 and 1650 m above sea level, and it ranges from 2200 to 5500 m in the Qilian Mountains. There are four major inland rivers in the study area, and all of them originate from Qilian Mountains, they are Shiyang River, Heihe River, Beida River, and Shule River from east to west. The Heihe River is located in E96°50′–102°00′, N37°50′–42°40′ and is the second largest inland river in China. It has a length of 948 km, a total drainage area of 142,900 km^2 and the mean annual discharge of 37.55×10^8 m^3, draining through Qinghai, Gansu and Inner Mongolia provinces. The eastern sub-river basin is the main river basin of the Heihe river system, has a drainage area of 116,000 km^2 and the mean annual discharge of 24.75×10^8 m^3. The Beida River is the largest tributary of Heihe River, flowing through Jiuquan County, and finally converges into the main channel at Jinta County. It has a length of 360 km, a drainage area of 6880 km^2 and a mean annual discharge of 6.53×10^8 m^3. The Shule River is the second largest river in this area, with a length of 670 km and a drainage basin area of 41,300 km^2 and a mean annual discharge of 15.13×10^8 m^3, it finally flows into Lop Nur area in Xinjiang Province. The Shiyang River has a length of 250 km, with an area of 41,600 km^2 and a mean annual discharge of 15.75×10^8 m^3, and drains into Qingtu Lake at the north of Minqin County.

As far from the coast, the study area is mainly dominated by an arid continental climate. In Qilian Mountains, the annual mean air temperature varies from −5 to 4 °C and the annual total precipitation averages at about 200 mm, and it increases to about 600–700 mm at higher altitudes. In contrast, the average annual temperature ranges from 5.8 to 10 °C in the plains area, and the precipitation decreases from southeast to northwest in the corridor, with 162 mm in Wuwei, 125 mm in Zhangye, and 86 mm in Jiuquan, while the potential evaporation ranges from 1900 to 3500 mm.

The study area transects three geological units, the Qilian Paleozoic geosynclinal fold zone, the Hexi Corridor depression and the Beishan tectonic belt. The uplift of the Qilian Mountains in the south has occurred since the end of the Paleozoic and has formed an active fold and thrust belt that extends along the northeastern margin of the Tibetan Plateau (Tapponnier et al. 1990; Meyer et al. 1998). The source areas and the upper reaches of these rivers are covered with Proterozoic high-grade metamorphic rocks, Paleozoic volcanic rocks, carbonate rocks, and clastic rocks and granitoids of different stages (Wu et al. 1993, 2004; Feng and He 1996; Yang et al. 2002; Song et al. 2004; Hou et al. 2006; Tseng et al. 2007; Zhang et al. 2007b). During the end of the Paleozoic and throughout the Mesozoic, the embryonic form of the Hexi Corridor was created. And then, from the late Tertiary, especially from the end of the Pliocene and the beginning of the early Pleistocene, intensive denudation and erosion from the Qilian Mountains led to significant transfer of clastic material to the basin depressions. During the following Quaternary, the clastic material in mountains was brought into the basins by water flows, forming the thick Quaternary aquifer of fluvial and alluvial sediments, and some aeolian and lacustrine deposits. The lower reaches of these rivers are mostly Quaternary alluvial–diluvial plains containing massive beds of loess, sand and gravel, and evaporites (mainly gypseous, mirabilite, halite) are widely distributed in this area.

Sampling and analytical methods

River water samples from mainstream and major tributaries of Heihe, Shule, Beida, and Shiyang River were collected in October 2012, and the sampling locations are shown in Fig. 1. Electric conductance (EC) and pH of the water samples were measured in the field. Alkalinity was titrated by using 0.010 M hydrochloric acid. Water samples was collected by using 10 L high density polyethylene (HDPE) containers, and immediately filtered through 0.22 μm

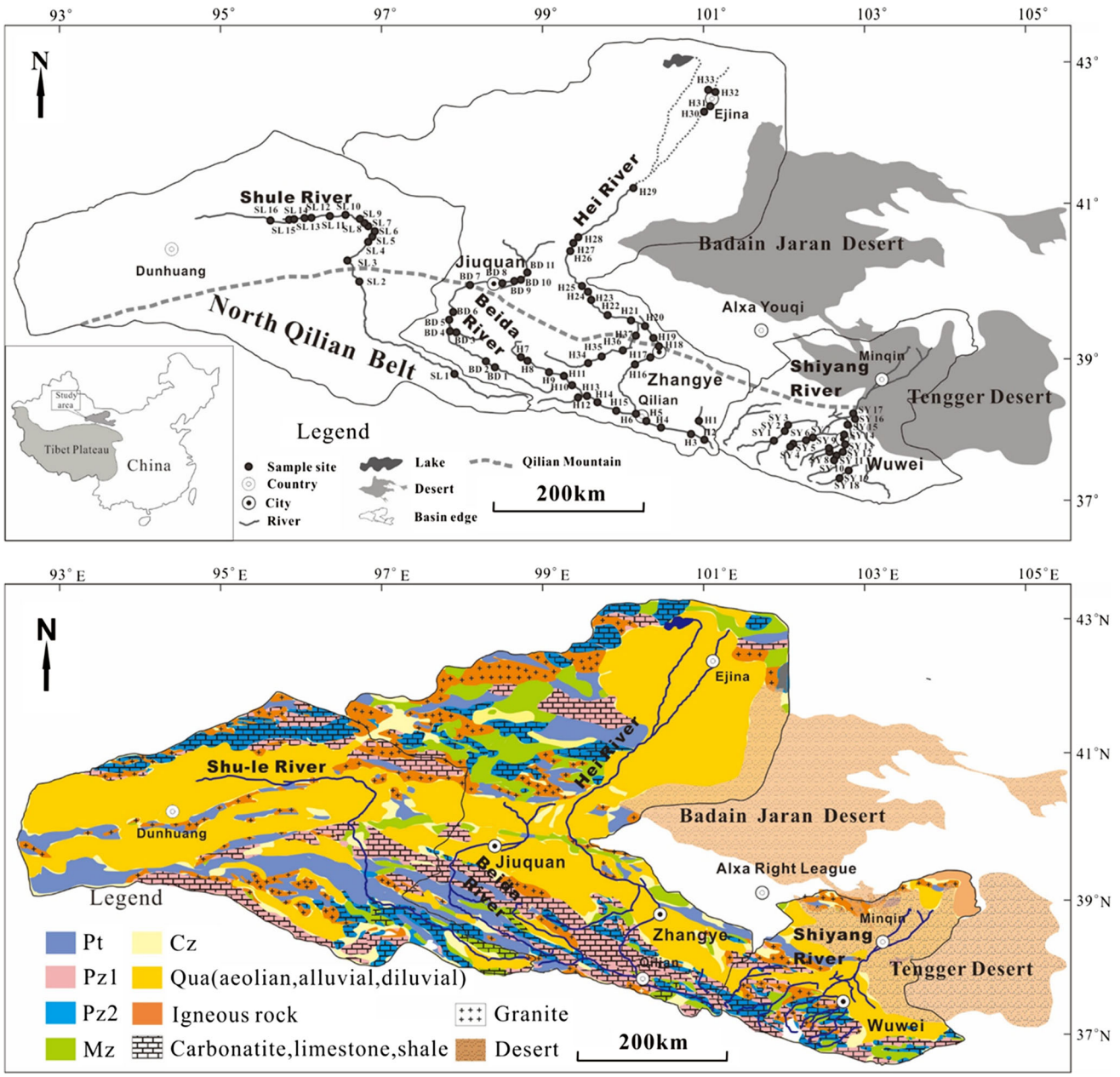

Fig. 1 Sampling sites and geologic map of the river basins around the Badain Jaran Desert. Ar, Pt, Pz1, Pz2, Mz, Cz, and Qua are the abbreviations of Archaean, Proterozoic, Early Paleozoic, Late Paleozoic, Mesozoic, Cenozoic, and Quaternary, respectively

Millipore membrane filters into a series of bottles for analysis. Five hundred milliliter filtration was acidified to pH < 1.6 with 6 M double sub-boiling distilled HNO_3 for cations and strontium determination. Fifty milliliter filtered water sample was stored directly in a polyethylene bottle for anion determination. Then, each bottle was screwed tightly and wrapped with para-film strip. All containers were previously washed with hydrochloric acid and rinsed with Milli-Q water (18.2 MΩ cm) and dried.

Anions (Cl^-, SO_4^{2-}, and NO_3^-) were measured by ionic chromatography (Dionex 120) with a precision of 5 %. Major cations (K^+, Na^+, Ca^{2+}, and Mg^{2+}) and Sr concentrations were determined by ICP–AES (IRIS Intrepid II, USA) with analytical precisions better than 5 %. Aqueous silica concentrations were determined by spectrophotometry using molybdate blue method. Reagent and procedural blanks were determined in parallel to the sample treatment. Each calibration curve was evaluated by analysis of the quality control (QC) standards before, during and after the analysis of a set of samples.

For the determination of the $^{87}Sr/^{86}Sr$ ratio, based on Sr concentration of each sample, a certain volume of water

sample was prepared by evaporating it to dryness in a Teflon vessel in ultraclean laboratory. The residue was then dissolved in double distilled 2.0 N HCl, and strontium in the solution was separated from matrix elements using a cation-exchange resin (Dowex 50 W × 8 200–400 mesh) in a quartz column by elution of 2.0 N HCl. The $^{87}Sr/^{86}Sr$ isotopic ratio was then analyzed with a VG-354 mass spectrometer with five Faraday collectors. The total blank was approximately 100 pg for the entire procedure. The reproducibility was verified by periodic determinations of the NBS 987 strontium standard. The average $^{87}Sr/^{86}Sr$ ratio of this standard for 25 determinations was 0.710236 ± 0.000012 (2σ, $n = 25$) during analysis.

Results and discussion

Major ion chemistry and Sr isotopes

The measured parameters (pH and EC), chemical and Sr isotopic compositions of water samples are presented in Table 1. Most of the water samples were alkaline with pH values ranging from 6.96 to 8.54, an average of 8.16. The extent of inorganic charge imbalance, characterized by the normalized inorganic charge balance (NICB = 100 × $(TZ^+ - TZ^-)/TZ^+$, where $TZ^+ = K^+ + Na^+ + 2Ca^{2+} + 2\,Mg^{2+}$, $TZ^- = HCO_3^- + Cl^- + NO_3^- + 2SO_4^{2-}$ in μEq), was generally less than ±10 %, indicating that the contribution of organic ligands to the charge balance was negligible. The total cationic charge (TZ^+) ranged between 3271 and 11,439 μEq, with an average of 7379 μEq, significantly higher than those of the global river average ($TZ^+ = 1125$ μEq, Meybeck 2003). The electric conductivity (EC) of the water samples varied from 303 to 952 μS cm^{-1}, which had a linear relationship with the total cationic charge measure in the rivers ($R^2 = 0.92$). The total dissolved solids (TDS) varied from 249 to 895 mg L^{-1}, with a mean value of 511 mg L^{-1}. The mean TDS values of Heihe, Shule, Beida, and Shiyang river waters were 546, 503, 486, and 459 mg L^{-1}, respectively. In comparing with other rivers worldwide (Gaillardet et al. 1999), these rivers in arid region are with significantly higher dissolved solid contents.

Variations of major ion compositions are shown in the cation and anion ternary diagram (Fig. 2). Ca^{2+} and Mg^{2+} were major cations in these rivers, with concentrations ranging from 732 to 2361 μmol L^{-1} and from 357 to 3016 μmol L^{-1}, respectively. They accounted for 59.7–94.4 % of the total cations (Fig. 2a). HCO_3^- was the dominant anion with concentrations ranging from 1830 to 6365 μmol L^{-1}. The next major anion SO_4^{2-} had concentrations ranging from 262 to 2637 μmol L^{-1}. HCO_3^- and SO_4^{2-} together accounted for 73.8–97 % of the total anions (Fig. 2b). There was no obvious difference in the chemical composition among the four rivers; however, some significant spatial changes can be observed along the river main channels. The Na^+, Cl^-, SO_4^{2-}, and TDS concentrations of Heihe, Shule, and Beida gradually increased from their upstream to downstream (Fig. 3a–d), indicating a contribution of evaporites dissolution and evaporation process in these inland rivers. Compared with other rivers and global average, the studied rivers are characterized by significant enriched Na^+, SO_4^{2-} and Cl^- in major ion compositions. The strontium concentrations of these rivers ranged from 2.16 to 13.0 μmol L^{-1}, with an average of 6.27 μmol L^{-1}. It is much higher than the global average value of 0.89 μmol L^{-1} estimated by Palmer and Edmond (1992). The Sr isotopic compositions ($^{87}Sr/^{86}Sr$) varied between 0.71019 and 0.71628, averaged at 0.71328. The $^{87}Sr/^{86}Sr$ ratio spatial evolution may reflect the geological setting of the river basin. In general, the upper reaches at the Qilian Mountains drain old terrains which consist mostly of metamorphic rocks, clastic rocks, and granitoids, show high $^{87}Sr/^{86}Sr$ ratios, whereas the lower reaches draining the Quaternary alluvial–diluvial plains have low $^{87}Sr/^{86}Sr$ ratios and high Sr concentrations. Taking the Shule River as an example, the Sr^{2+} concentrations and $^{87}Sr/^{86}Sr$ ratio evolution along the Shule main channel are shown in Fig. 3e.

Source of solutes

Atmospheric and anthropogenic inputs

The solutes of river waters are generally products of rocks and minerals weathering, dry and wet atmospheric deposition, and anthropogenic inputs. In order to determine the dissolved load deriving from rock weathering, the first step is to correct for atmospheric and anthropogenic input. The products of human activities go into river water by waste input, such as agricultural fertilizers, animal waste, and municipal and industrial sewage. The contribution of the anthropogenic source to these rivers could be ignored in this study as the lack of human activities in the desert regions. The atmospheric input contains two principal components: marine and soil dust. As these inland rivers are far away from the ocean, it is reasonable to argue that they may not be significantly influenced in chemical composition by marine inputs. The soil dust input might be important due to the poor covering of vegetation in marginal areas of the desert, and most solids in the soil dust are salinized and enriched in soluble cations. However, the contribution of the soil dust input could be regarded as a part of rock weathering (Zhang et al. 1995b). Therefore, the influence of the marine and anthropogenic inputs on the dissolved load of the rivers in this study is negligible.

Table 1 Chemical and strontium isotope compositions of rivers around the Badain Jaran Desert

Sample no.	pH	EC (μs/cm)	K^+ (μmol L^{-1})	Na^+ (μmol L^{-1})	Ca^{2+} (μmol L^{-1})	Mg^{2+} (μmol L^{-1})	HCO_3^- (μmol L^{-1})	Cl^- (μmol L^{-1})	SO_4^{2-} (μmol L^{-1})
Heihe River									
HH-1	8.41	919	81	1024	2159	3007	5287	309	2636
HH-2	8.44	652	165	2119	1135	1849	6239	280	534
HH-3	8.53	754	178	3161	1012	1467	6365	539	778
HH-4	8.30	667	84	1359	1681	1893	4654	241	1445
HH-5	8.31	698	84	1177	1988	2006	4548	262	1728
HH-6	8.23	606	73	818	1647	1963	4538	203	1478
HH-7	8.10	522	55	577	1941	836	4591	179	668
HH-8	7.85	564	56	769	1846	895	3567	668	890
HH-9	7.77	539	53	788	1593	1432	4301	723	853
HH-10	8.53	327	38	333	1006	572	2702	230	262
HH-11	8.42	399	43	329	1236	1139	3476	196	616
HH-12	8.39	565	75	754	1746	1581	4953	204	1074
HH-13	8.23	581	79	763	1683	1737	5036	197	1123
HH-14	8.46	563	67	672	1632	1787	4654	209	1196
HH-15	8.41	611	71	783	1678	2006	4581	194	1525
HH-16	8.28	608	75	872	1719	1958	3967	240	1680
HH-17	8.26	601	73	854	1828	1998	4304	230	1589
HH-18	8.28	591	76	885	1471	1955	3736	233	1564
HH-19	8.42	657	106	1221	1528	1981	3960	511	1431
HH-20	7.88	580	109	1259	1674	2214	4895	494	1399
HH-21	8.48	658	106	1297	1576	2143	4631	530	1415
HH-22	8.07	632	113	1576	785	2403	3721	631	1479
HH-23	7.63	696	114	1677	813	2401	3924	712	1571
HH-24	7.52	717	111	1749	1646	1765	4277	743	1584
HH-25	7.55	735	119	1843	1223	1749	3859	841	1708
HH-26	8.53	751	133	1973	1516	1823	3625	936	1754
HH-27	8.45	725	125	1890	1531	1754	4214	924	1852
HH-28	7.30	734	132	1923	837	1806	3021	920	1839
HH-29	7.56	760	153	2224	834	1968	3031	1094	2080
HH-30	8.54	787	164	2408	805	2126	3356	1179	2142
HH-31	8.44	809	171	2507	1303	2246	3480	1188	2119
HH-32	7.24	816	169	2480	1115	1948	3433	1230	2181
HH-33	7.16	825	159	2317	1186	2098	3523	1239	2180
HH-34	8.23	565	65	726	835	1893	3313	302	1344

Table 1 continued

Sample no.	pH	EC (μs/cm)	K^+ (μmol L^{-1})	Na^+ (μmol L^{-1})	Ca^{2+} (μmol L^{-1})	Mg^{2+} (μmol L^{-1})	HCO_3^- (μmol L^{-1})	Cl^- (μmol L^{-1})	SO_4^{2-} (μmol L^{-1})
HH-35	7.98	559	67	929	1551	2010	4410	370	1318
HH-36	8.22	655	81	1782	901	1715	3228	1096	1415
HH-37	8.41	551	82	1086	867	1752	3011	443	1273
Shule River									
SL-1	8.29	489	53	1061	1021	1391	3871	719	414
SL-2	8.14	650	84	1523	782	2349	3480	1237	1365
SL-3	8.26	545	73	1180	783	1877	2948	897	1113
SL-4	8.3	542	74	1222	774	1863	2924	872	1092
SL-5	8.29	539	71	1175	1156	1873	3880	865	1084
SL-6	8.42	584	111	1264	1148	2081	4160	923	1123
SL-7	8.22	594	84	1274	1238	2078	4260	979	1206
SL-8	8.06	602	89	1392	786	2146	3093	1018	1246
SL-9	8.41	725	111	1887	1417	1743	3166	1657	1711
SL-10	8.40	624	92	1455	1298	2258	4320	1217	1376
SL-11	8.47	657	98	1660	1004	2404	3650	1369	1528
SL-12	8.38	664	118	1728	1329	2425	3811	1356	1762
SL-13	8.35	668	112	1628	1289	2343	3726	1363	1763
SL-14	8.36	704	117	1753	1281	2354	3440	1487	1897
SL-15	8.36	701	116	1562	1205	2200	3244	1299	1674
SL-16	8.34	744	127	1930	1407	1761	2745	1493	1915
Beida River									
BD-1	8.32	441	60	390	1418	709	2890	273	697
BD-2	8.08	461	66	275	1429	1418	3570	139	941
BD-3	8.22	511	45	514	1234	2019	4054	344	1141
BD-4	8.45	476	47	605	1145	1656	3630	281	993
BD-5	8.07	469	69	511	1161	1128	3100	287	792
BD-6	8.16	582	76	594	953	2283	2958	365	1683
BD-7	8.15	480	67	507	815	1848	3349	301	939
BD-8	7.93	456	100	583	732	1586	3103	351	854
BD-9	7.65	715	239	1722	1296	2337	4598	1107	1224
BD-10	7.30	952	247	2074	1425	3016	4616	1305	2637
Shiyang River									
SY-1	8.13	530	43	516	1897	1393	3938	96	1380
SY-2	8.29	453	45	524	1106	819	1977	112	1150
SY-3	8.05	870	99	2751	1643	1987	3364	1602	2234

Table 1 continued

Sample no.	pH	EC (μs/cm)	K^+ (μmol L^{-1})	Na^+ (μmol L^{-1})	Ca^{2+} (μmol L^{-1})	Mg^{2+} (μmol L^{-1})	HCO_3^- (μmol L^{-1})	Cl^- (μmol L^{-1})	SO_4^{2-} (μmol L^{-1})
SY-4	8.19	515	34	323	1032	1509	2982	79	1390
SY-5	8.33	529	39	353	1217	885	1830	96	1479
SY-6	8.35	518	38	336	1909	802	2827	101	1375
SY-7	8.32	502	43	411	1864	773	2837	121	1289
SY-8	8.44	315	42	327	1120	384	2160	127	363
SY-9	8.42	312	36	506	1131	373	2030	202	509
SY-10	8.54	497	78	659	1005	734	1920	255	964
SY-11	8.48	434	43	373	1583	617	2697	100	939
SY-12	8.54	424	55	416	1595	562	2706	141	885
SY-13	8.38	303	40	380	1068	357	2083	151	419
SY-14	6.96	952	558	2912	2361	718	4994	2163	899
SY-15	8.02	932	256	1949	1713	1909	4280	1442	1576
SY-16	7.03	726	123	1700	1986	1614	4594	1194	1260
SY-17	7.94	584	76	1570	1472	804	3286	1132	898

Sample no.	NO_3^- (μmol L^{-1})	F^- (μmol L^{-1})	SiO_2 (μmol L^{-1})	TDS (mg L^{-1})	TZ+ (μEq)	TZ- (μEq)	NICB[a] (%)	Sr (μmol L^{-1})	$^{87}Sr/^{86}Sr$	2σ
Heihe River										
HH-1	155	6	79	787	11,439	11030	3.6	7.77	0.713908	12
HH-2	103	7	88	599	8253	7699	6.7	3.30		
HH-3	118	10	86	651	8296	8588	−3.5	4.79	0.712345	13
HH-4	73	8	99	590	8589	7867	8.4	7.90		
HH-5	75	9	102	604	9250	8351	9.7	8.26	0.711443	12
HH-6	61	9	116	511	8110	7767	4.2	5.50		
HH-7	20	4	133	473	6187	6131	0.9	3.66	0.710186	12
HH-8	99	6	90	454	6307	6119	3.0	4.05	0.711433	11
HH-9	58	6	80	436	6891	6794	1.4	3.85		
HH-10	65	5	133	274	3526	3526	0.0	2.16	0.712668	12
HH-11	81	6	132	341	5123	4991	2.6	2.59		
HH-12	45	12	100	489	7482	7361	1.6	4.04	0.715335	10
HH-13	44	13	103	500	7682	7536	1.9	4.03		
HH-14	51	9	120	483	7577	7314	3.5	3.70		
HH-15	58	9	112	519	8221	7891	4.0	5.16	0.713537	13
HH-16	107	8	106	540	8300	7682	7.5	6.28	0.712789	8
HH-17	134	33	139	536	8580	7880	8.2	6.20		

Table 1 continued

Sample no.	NO_3^- (μmol L^{-1})	F^- (μmol L^{-1})	SiO_2 (μmol L^{-1})	TDS (mg L^{-1})	TZ+ (μEq)	TZ- (μEq)	NICB[a] (%)	Sr (μmol L^{-1})	$^{87}Sr/^{86}Sr$	2σ
HH-18	89	10	114	510	7814	7195	7.9	6.24		
HH-19	188	11	149	493	8344	7532	9.7	7.01	0.712884	8
HH-20	726	31	158	556	9142	8945	2.2	7.37		
HH-21	207	10	107	533	8840	8208	7.1	7.34		
HH-22	217	15	158	545	8065	7543	6.5	7.21	0.712861	12
HH-23	218	10	163	573	8220	8006	2.6	7.42		
HH-24	179	11	164	614	8682	8377	3.5	8.09	0.712887	9
HH-25	193	11	156	610	7907	8320	−5.2	7.90		
HH-26	183	10	166	600	8785	8261	6.0	8.24		
HH-27	185	9	157	641	8584	9035	−5.3	8.14	0.712895	14
HH-28	198	10	161	585	7341	7828	−6.6	7.72		
HH-29	182	11	169	608	7981	8477	−6.2	8.51	0.712904	13
HH-30	192	13	173	629	8434	9023	−7.0	8.27		
HH-31	168	13	196	651	9776	9086	7.1	9.17	0.712885	12
HH-32	169	13	184	642	8774	9207	−4.9	9.12		
HH-33	228	36	187	652	9044	9386	−3.8	8.58		
HH-34	183	24	95	480	6247	6509	−4.2	4.58	0.712861	13
HH-35	485	35	99	532	8118	7935	2.3	4.98		
HH-36	172	5	99	510	7096	7331	−3.3	6.92		
HH-37	118	6	70	439	6406	6124	4.4	5.49	0.712719	10
Shule River										
SL-1	29	6	111	411	5937	5452	8.2	3.83	0.712911	10
SL-2	62	12	108	524	7869	7520	4.4	5.40	0.713236	10
SL-3	61	11	103	436	6573	6143	6.5	4.57	0.713509	9
SL-4	58	1	98	431	6570	6048	7.9	4.66	0.712641	11
SL-5	56	10	102	446	7303	6979	4.4	4.70		
SL-6	73	12	104	456	7833	7415	5.3	5.19		
SL-7	77	12	107	486	7989	7741	3.1	5.21		
SL-8	92	13	114	476	7345	6708	8.7	5.24		
SL-9	97	13	112	576	8319	8353	−0.4	6.46	0.713367	10
SL-10	79	13	107	517	8658	8381	3.2	5.58		
SL-11	86	12	117	535	8574	8173	4.7	6.05	0.713284	11
SL-12	85	15	110	551	9352	8791	6.0	7.23		
SL-13	73	15	108	546	9003	8705	3.3	6.86	0.713059	10
SL-14	69	15	122	567	9138	8805	3.7	7.07		

Table 1 continued

Sample no.	NO_3^- (μmol L^{-1})	F^- (μmol L^{-1})	SiO_2 (μmol L^{-1})	TDS (mg L^{-1})	TZ+ (μEq)	TZ- (μEq)	NICB[a] (%)	Sr (μmol L^{-1})	$^{87}Sr/^{86}Sr$	2σ
SL-15	55	13	110	520	8488	7959	6.2	6.96		
SL-16	71	15	117	564	8392	8155	2.8	7.45	0.713014	10
Beida River										
BD-1	51	9	110	369	4703	4617	1.8	2.45	0.715352	11
BD-2	52	6	65	397	6035	5648	6.4	2.60		
BD-3	60	5	82	429	7064	6746	4.5	3.13		
BD-4	63	5	118	403	6254	5966	4.6	2.46	0.715590	11
BD-5	72	18	121	549	5158	5061	1.9	2.54		
BD-6	95	8	119	478	7141	6792	4.9	3.67	0.715637	9
BD-7	90	9	149	428	5901	5627	4.6	2.98	0.715561	12
BD-8	167	33	131	408	5320	5362	−0.8	2.96		
BD-9	560	43	157	609	9229	8757	5.1	3.93		
BD-10	135	22	227	791	11,203	11,351	−1.3	11.02	0.713578	12
Shiyang River										
SY-1	103	4	105	470	7139	6901	3.3	13.01		
SY-2	119	4	85	387	4418	4511	−2.1	10.36		
SY-3	185	27	97	676	10,111	9647	4.6	12.37	0.713368	11
SY-4	116	5	93	439	5438	5961	−9.6	6.47	0.716284	11
SY-5	106	8	94	417	4597	4999	−8.8	8.43		
SY-6	106	8	91	425	5795	5793	0.0	7.84	0.714246	10
SY-7	97	10	87	417	5728	5644	1.5	7.49		
SY-8	155	19	74	249	3376	3189	5.5	2.55		
SY-9	127	16	76	260	3550	3393	4.4	6.56	0.711036	12
SY-10	211	9	95	394	4216	4323	−2.5	7.19		
SY-11	106	8	80	358	4817	4789	0.6	7.80	0.713480	11
SY-12	127	9	79	357	4787	4752	0.7	7.15		
SY-13	177	22	65	250	3271	3270	0.0	4.17	0.711683	17
SY-14	236	10	243	895	9628	9202	4.4	8.59		
SY-15	1177	12	227	781	9448	10,063	−6.5	12.67	0.712597	11
SY-16	0	13	159	566	9024	8322	7.8	9.77		
SY-17	29	23	146	455	6199	6265	−1.1	7.34	0.711532	10

[a] $NICB = 100 \times (TZ^+ - TZ^-)/TZ^+$

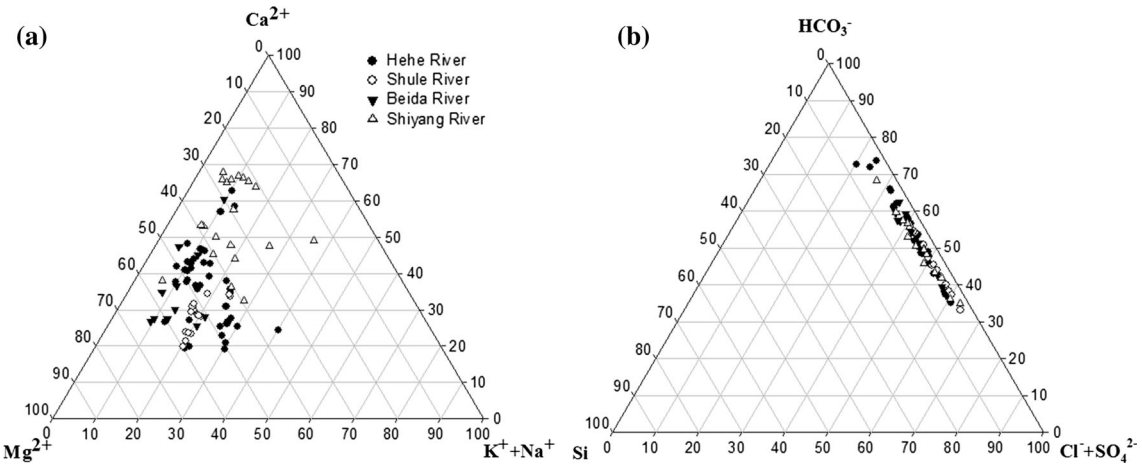

Fig. 2 Ternary diagrams for the cations (**a**) and anions (**b**) in the rivers around the Badain Jaran Desert

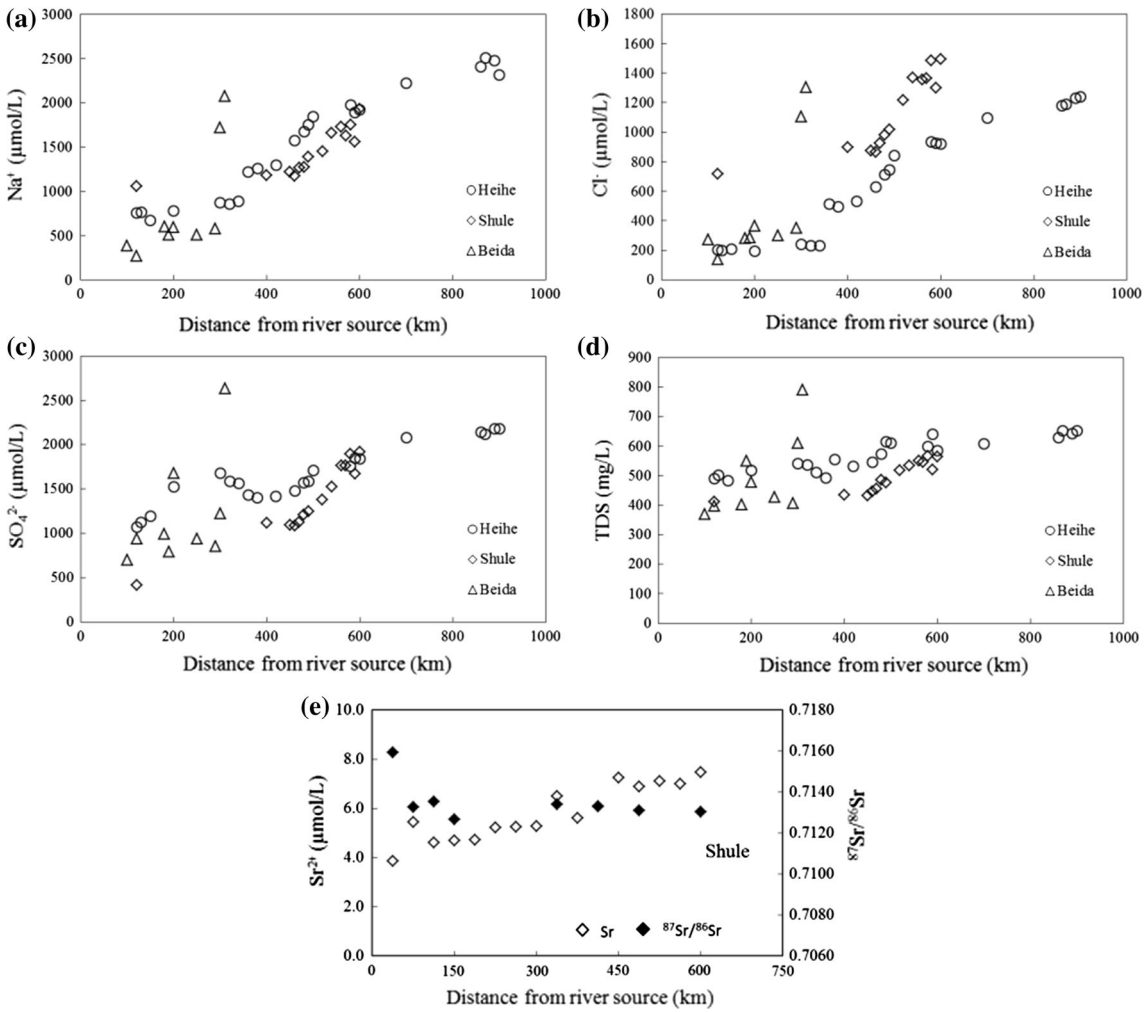

Fig. 3 Na^+ (**a**), Cl^- (**b**), SO_4^{2-} (**c**), TDS (**d**), and Sr^{2+} and $^{87}Sr/^{86}Sr$ ratios (**e**) variation along the Heihe, Shule, and Beida river main channels from upstream to downstream

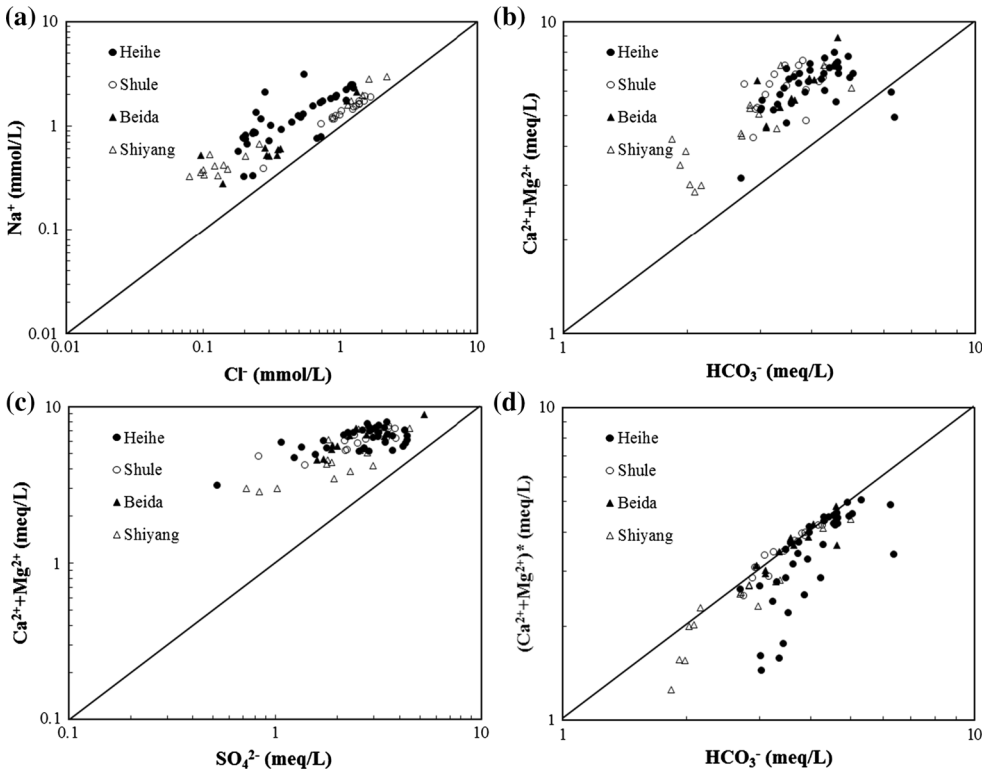

Fig. 4 Correlation between of major ionic composition for the river waters around the Badain Jaran Desert

Rock weathering inputs

Stoichiometric analysis would provide some qualitative information for tracing sources of major elements in river waters (Fig. 4). Halite (NaCl) are the most common evaporites in the arid regions. These rivers show significantly high Na^+ and Cl^- concentrations and a positive correlation between them ($R^2 = 0.78$, $n = 78$, except for two samples in the upper Heihe), and display a trend toward the 1:1 line at high concentrations for both constituents (Fig. 4a). As the influence from sea salt is weak in these inland rivers, halite dissolution should be a dominant source of Na^+ and Cl^- in the rivers. Most river water samples have equivalent ratios of Na^+/Cl^- larger than one, presumably indicating sources of Na^+ from dissolution of mirabilite ($Na_2SO_4{\cdot}10H_2O$) and/or silicate weathering. However, there is no strong correlation between Na^+ and SO_4^{2-} ($R^2 = 0.28$, $n = 80$), implying that contribution from mirabilite is not significant. The sources of Ca^{2+} and Mg^{2+} can be determined from the $(Ca^{2+} + Mg^{2+})/HCO_3^-$ equivalent ratio. Figure 4b shows that most samples have the $(Ca^{2+} + Mg^{2+})/HCO_3^-$ ratio larger than one, the excess of Ca^{2+} and Mg^{2+} over HCO_3^- reflects extra sources of Ca^{2+} and Mg^{2+} and is balanced by SO_4^{2-}. Most of river waters have high concentrations of Ca^{2+}, Mg^{2+} and SO_4^{2-} in the studied area. Gypsum ($CaSO_4{\cdot}H_2O$) and other composite sulfates of Ca, Mg, Na, and K (e.g. bloedite, anhydrite) may be also widely distributed in the desert areas (Zhang et al. 1995b). However, water samples have equivalent ratios of $(Ca^{2+} + Mg^{2+})/SO_4^{2-}$ larger than one and show significant excess in Ca^{2+} and Mg^{2+} (Fig. 4c). The excess of Ca^{2+} and Mg^{2+} over SO_4^{2-} could suggest an additional supply by the weathering of both silicate and/or carbonate rocks. In the source area and upper reaches of these inland rivers, metamorphic rocks, carbonate rocks, clastic rocks, and granitoids of different stages are exposed on the earth surface; meanwhile, Quaternary deposits are widely distributed in the middle and lower reaches, which contains some carbonate as well. We calculated the excess of $(Ca^{2+} + Mg^{2+})^*$ by subtracting SO_4^{2-} from the total Ca^{2+} and Mg^{2+} in river waters ($(Ca^{2+} + Mg^{2+})^* = (Ca^{2+} + Mg^{2+}) – SO_4^{2-}$), and the variation of $(Ca^{2+} + Mg^{2+})^*$ with HCO_3^- in Fig. 4d is used to understand the weathering of carbonate and/or silicate rocks. If the excess of Ca^{2+} and Mg^{2+} are mainly from the weathering of carbonate, the $(Ca^{2+} + Mg^{2+})^*$ and HCO_3^- should display a trend on the 1:1 line. Some samples from the Shule and Beida are closer to the equivalent line (Fig. 4d), and the other samples have $(Ca^{2+} + Mg^{2+})^*/HCO_3^-$ ratios significantly <1, indicating an additional >amount of Na^+ and K^+ which may be derived from the weathering of silicate rocks to balance the excess of HCO_3^-.

Strontium isotopic composition ($^{87}Sr/^{86}Sr$) of river water directly reflects that of the parent rock releasing as it is not fractionated during weathering processes and

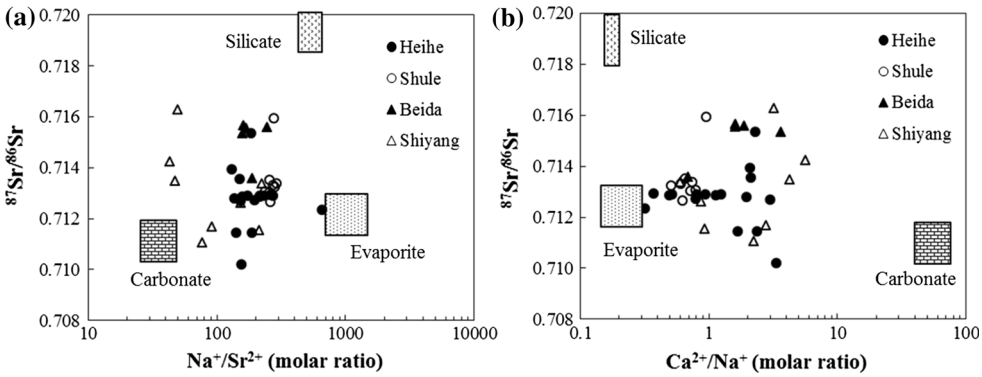

Fig. 5 Correlation between $^{87}Sr/^{86}Sr$ and Na^+/Sr^{2+} (**a**) and Ca^{2+}/Na^+ (**b**) molar ratios of the river waters around the Badain Jaran Desert

Table 2 Elemental and Sr isotopic ratios of H_2O-soluble minerals (evaporites) and acid-insoluble minerals (silicates) from sand sample collected at the Badain Jaran Desert and its surrounding areas

Location	Evaporite					Silicate				
	K/Na	Ca/Na	Mg/Na	Sr/Na	$^{87}Sr/^{86}Sr$	K/Na	Ca/Na	Mg/Na	Sr/Na	$^{87}Sr/^{86}Sr$
Badain Jaran[a]	–	0.59	0.32	0.0021	0.71278	–	–	–	–	0.71536
Badain Jaran[c]	–	–	–	–	0.71268	–	–	–	–	0.71986
Tengger[b]	0.40	2.59	0.38	0.0095	0.7113	0.66	0.19	0.18	0.0026	0.72157
Dunhuang[a]	–	15.6	0.66	0.0289	0.71196	–	–	–	–	0.71510
Yanchi[b]	0.87	7.86	0.56	0.0128	0.71158	0.19	0.25	0.31	0.0025	0.71867

[a] Data are from Yokoo et al. (2001)

[b] Data are from Yokoo et al. (2004)

[c] Data are from Nakano et al. (2004)

independent of dilution and evaporation effects. Therefore, $^{87}Sr/^{86}Sr$ ratios are often applied to identify the end-members of rock weathering in a watershed (Négrel et al. 1993; Zhang et al. 1995b; Gaillardet et al. 1999; Millot et al. 2003; Xu and Liu 2007). Based on the lithology of the studied area, the headwater drainage areas on northern foot of the Qilian Mountains are covered with Proterozoic high-grade metamorphic rocks and Paleozoic sedimentary rocks. Radiogenic strontium is supposed to be enriched in these rocks, resulting in high $^{87}Sr/^{86}Sr$ ratios in the headwater of rivers. However, the low reaches of rivers draining Quaternary alluvial plains and desert areas have low $^{87}Sr/^{86}Sr$ ratios. The relationships between $^{87}Sr/^{86}Sr$ and Na^+/Sr^{2+} and Ca^{2+}/Na^+ molar ratios of these rivers are presented in Fig. 5. It shows that different mixing trends of at least three end-members for rivers, which are evaporite, carbonate, and silicate. The geochemical characteristics of these end-members can be deduced from the correlations between $^{87}Sr/^{86}Sr$ and elemental ratios.

Desert sand and arid soils are composed of a mixture of salinization minerals and other minerals derived from provenance rocks and their weathered materials. Therefore, the $^{87}Sr/^{86}Sr$ and ion concentration ratios of the different rock weathering source for these rivers could be well defined by those of various minerals in surface soil in the drainage basin. Yokoo et al. (2001) reported elemental and Sr isotopic composition of the H_2O-soluble fraction from sand samples collected at the Badain Jaran Desert. Their chemical and X-ray diffraction (XRD) analysis showed that evaporite minerals (mainly halite and gypsum) were dissolved in the H_2O-soluble fraction, and consequently, these elemental and Sr isotopic ratios ($Ca/Na = 0.59$, $Mg/Na = 0.32$, $1000 \times Sr/Na = 2.13$, and $^{87}Sr/^{86}Sr = 0.712782$) may represent the evaporite end-member composition. Nakano et al. (2004) also reported the H_2O-soluble minerals have $^{87}Sr/^{86}Sr$ ratios of 0.712680 of desert sand in the Badain Jaran Desert. They also determined the elemental and $^{87}Sr/^{86}Sr$ compositions of the acid-insoluble minerals in surface soil and/or sand from the Badain Jaran Desert and its surrounding areas (Yokoo et al. 2001, 2004; Nakano et al. 2004), and the ratios are presented in Table 2.

Identification of silicate end-member composition is difficult because silicate rocks show variable $^{87}Sr/^{86}Sr$ ratios and their Sr isotopic compositions are controlled by the types and ages of the rocks. A recent research shows that the aeolian deposits in the Badain Jaran Desert are predominantly derived from the Qilian Mountains (Hu and Yang 2016), and geochemical composition of the aeolian

sand samples indicates these sediments should be mainly derived from mixed source rocks of granite, granitoids, and granodiorite. Therefore, the chemical and Sr isotopic compositions of the silicate fractions in the desert sand could be more representative of the mean composition of the silicate end-member in the drainage basin area. Yokoo et al. (2001) determined Sr isotopic ratios (0.715360) of acid-insoluble minerals (silicates) in sand sample from the Badain Jaran Desert. Chen et al. (2007) also reported that Sr isotopic compositions of the fine-grained silicate fractions (<75 μm) of the surface sand in the desert are quite homogeneous, with an average of 0.716243. According to Nakano et al. (2004), the acid-insoluble minerals have $^{87}Sr/^{86}Sr$ ratios of 0.719864 in the Badain Jaran Desert. Unfortunately, they did not report the elemental compositions of the acid-insoluble minerals in surface soil and/or sand from the Badain Jaran Desert. Yokoo et al. (2004) determined the elemental compositions of acid-insoluble minerals in sand sample from the Tengger Desert, which is adjacent to the Badain Jaran Desert. In this paper, we adopt the elemental ratio values reported by Yokoo et al. (2004) as the silicate weathering end-members for the studied rivers (Table 2). Identification of carbonate end-member compositions by river waters is not easy because there are both weathering input of the primary carbonate and the dissolution of carbonate formed by evaporation in arid soil (Yokoo et al. 2001). We adopt the values for carbonate end-member suggested by Wu et al. (2005) in the case of the upper Huanghe River basin which is close to our study area, with 60 ± 30, 17 ± 11, 65 ± 30, and 0.71050 ± 0.0005 for Ca/Na, Mg/Na, $1000 \times$ Sr/Na, and $^{87}Sr/^{86}Sr$ ratios, respectively.

Chemical budget and rock weathering sources to river water

To estimate the contribution of the different sources to the river water, a forward method is employed in this study. The mass budget equation for any element X (Cl^-, SO_4^{2-}, Na^+, K^+, Ca^{2+}, and Mg^{2+}) in the dissolved load can be written as:

$$[X]_{riv} = [X]_{atm} + [X]_{anth} + [X]_{eva} + [X]_{carb} + [X]_{sil} \quad (1)$$

where *riv* river water, *atm* atmospheric input, *anth* anthropogenic input, *sil* silicate, *carb* carbonate, *eva* evaporite.

The calculation is based on some straightforward simplifications of the budget equations. As discussed above, anthropogenic and atmospheric inputs to the river water in this study are negligible. All Cl^- in rivers are assumed deriving from evaporite (mainly halite), and balanced by Na^+. All SO_4^{2-} in rivers are also assumed deriving from evaporites, and balanced by Ca^{2+} and Mg^{2+}. In addition, it is assumed that all K^+ are of silicate origin. K_{sil} might be overestimated in the area due to the existence of potassium salt (e.g. sylvites). However, as the concentration of K^+ accounts for less than 2 % of the total cations in river waters, the uncertainty caused by the assumption that all K^+ originates from silicates would be very small. The residual calcium and magnesium are attributed to the carbonate weathering. With these assumptions, the above equation can be simplified as follows:

$$[Cl]_{riv} = [Cl]_{eva} \quad (2)$$

$$[SO_4]_{riv} = [SO_4]_{eva} \quad (3)$$

$$[Na]_{riv} = [Cl]_{eva} + [Na]_{sil} \quad (4)$$

$$[SO_4]_{eva} = [Ca]_{eva} + [Mg]_{eva} \quad (5)$$

$$[K]_{riv} = [K]_{sil} \quad (6)$$

$$[Ca]_{riv} = [Ca]_{eva} + [Ca]_{carb} + [Ca]_{sil} \quad (7)$$

$$[Mg]_{riv} = [Mg]_{eva} + [Mg]_{carb} + [Mg]_{sil} \quad (8)$$

The proportional contribution of each reservoir to the dissolved cation load (K^+, Na^+, Ca^{2+}, and Mg^{2+}) of the river waters can be calculated. The calculated contributions of different sources to the dissolved cation load for these rivers around the Badain Jaran Desert are illustrated in Fig. 6. Overall, the dissolved cation load of rivers is dominated by evaporite dissolution and carbonate weathering. The contribution of evaporite and carbonate weathering accounts for about 80 % of the total dissolved cations for these rivers. The proportion of the dissolved cations from silicates weathering ($XCat_{sil}$) is 4–65, 8–15, 7–19 and 12–26 %, with an average of 23.5, 10.8, 12.1 and 18.2 % for Heihe, Shule, Beida, and Shiyang River, respectively. The contribution of carbonate weathering to the total dissolved cation load ($XCat_{car}$) accounts for 34.6 %

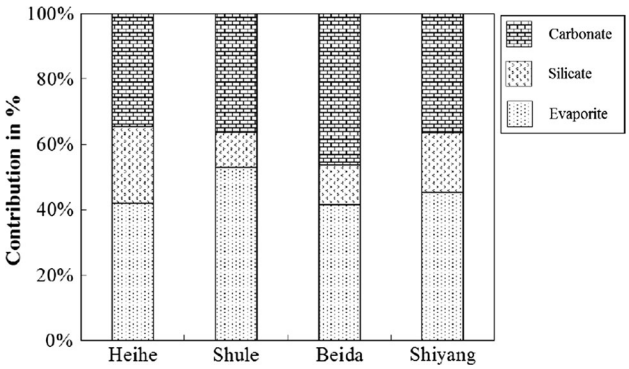

Fig. 6 Calculated contributions (in %) of the different reservoirs to the total dissolved cation load for the rivers around the Badain Jaran Desert. Evaporite dissolution and carbonate weathering dominated in these rivers

Table 3 Chemical weathering rates for the rivers around the Badain Jaran Desert

River	Discharge	Area	Source of Cations			Silicate		Carbonate		Evaporite	Total rock
	(10^8 m^3/years)	(km^2)	Eva.	Sil. %	Carb.	SWR[a] t km^{-2} a^{-1}	$Cation_{sil}$[b] t km^{-2} a^{-1}	CWR[a] t km^{-2} a^{-1}	$Cation_{carb}$[b] t km^{-2} a^{-1}	t km^{-2} a^{-1}	TWR[a] t km^{-2} a^{-1}
Heihe	24.75	116,000	41.9	23.5	34.6	0.81	0.64	1.91	0.93	1.27	3.99
Shule	15.13	41,300	53.0	10.8	36.2	0.76	0.52	3.48	1.61	1.76	6.0
Beida	6.53	6883	41.6	12.1	46.3	2.04	1.31	9.23	4.46	3.84	15.1
Shiyang	15.75	41,600	45.3	18.2	36.5	0.93	0.68	2.89	1.53	1.46	5.3

[a] SWR, CWR, and TWR represent silicate weathering rate, carbonate weathering rate, and total rock weathering rates, respectively

[b] $Cation_{sil}$ and $Cation_{carb}$ the sum of cation concentrations derived from silicate weathering and carbonate weathering

(10–66 %), 36.2 % (21–53 %), 46.3 % (25–58 %), and 36.5 % (15–57 %), and the contribution of evaporite dissolution to the dissolved cation load ($X\mathrm{Cat}_{\mathrm{eva}}$) is 41.9 % (15–61 %), 53.0 % (32–65 %), 41.6 % (34–58 %), and 45.3 % (26–63 %) for Heihe, Shule, Beida, and Shiyang River, respectively.

To test the sensitivity of our calculation, a model constituted of mass budget equations of Sr/Na molar ratios and Sr isotopic ratios is employed for comparison.

For Sr concentration, the mass balance equation can be written as:

$$(\mathrm{Sr/Na})_{\mathrm{riv}} = \alpha(\mathrm{Na}) \times (\mathrm{Sr/Na})_{\mathrm{eva}} + \beta(\mathrm{Na}) \times (\mathrm{Sr/Na})_{\mathrm{sil}} + \gamma(\mathrm{Na}) \times (\mathrm{Sr/Na})_{\mathrm{car}} \quad (9)$$

And for the Sr isotopic composition, the mixing equation can be written as:

$$\left(^{87}\mathrm{Sr}/^{86}\mathrm{Sr}\right)_{\mathrm{riv}} \times (\mathrm{Sr/Na})_{\mathrm{riv}} = \alpha(\mathrm{Na}) \times \left(^{87}\mathrm{Sr}/^{86}\mathrm{Sr}\right)_{\mathrm{eva}} \times (\mathrm{Sr/Na})_{\mathrm{eva}} + \beta(\mathrm{Na}) \times \left(^{87}\mathrm{Sr}/^{86}\mathrm{Sr}\right)_{\mathrm{sil}} \times (\mathrm{Sr/Na})_{\mathrm{sil}} + \gamma(\mathrm{Na}) \times \left(^{87}\mathrm{Sr}/^{86}\mathrm{Sr}\right)_{\mathrm{car}} \times (\mathrm{Sr/Na})_{\mathrm{car}} \quad (10)$$

And $\alpha + \beta + \gamma = 1$.

The fraction of Na from each end-member is denoted by α(Na), β(Na), and γ(Na). The results show that the proportion of the dissolved cations from silicates weathering is 13.6, 30.0, 10.4, and 13.0 % for Heihe, Shule, Beida, and Shiyang River, respectively. The propagated errors for the different XCat (in mean) are 20 % for silicate, 10 % for evaporites one, and 25 % for carbonate. For the calculation of the proportion of the contributions, the major source of uncertainties is the composition of the different end-members. The difference between contributions of each source estimated from Sr isotopes and the forward model can be attributed to the uncertainty of carbonate end-member composition.

The chemical weathering rate of rocks can then be estimated by the mass budget and the surface area and water discharges of the basin, expressed in ton km^{-2} a^{-1}. The rate of silicate weathering (SWR) is calculated using the Na, K, Ca, and Mg concentrations from silicate weathering and assumes that all dissolved SiO_2 is derived from the weathering of silicates.

$$\mathrm{SWR} = \left([\mathrm{Na}]_{\mathrm{sil}} + [\mathrm{K}]_{\mathrm{sil}} + [\mathrm{Ca}]_{\mathrm{sil}} + [\mathrm{Mg}]_{\mathrm{sil}} + [\mathrm{SiO_2}]_{\mathrm{riv}}\right) \times \mathrm{discharge/area} \quad (11)$$

The rate of carbonate weathering (CWR) is calculated using the dissolved Ca and Mg from carbonate weathering and HCO_3, with half of the HCO_3 from carbonate dissolution being derived from the atmosphere.

$$\mathrm{CWR} = \left([\mathrm{Ca}]_{\mathrm{carb}} + [\mathrm{Mg}]_{\mathrm{carb}} + 1/2[\mathrm{HCO_3}]_{\mathrm{carb}}\right) \times \mathrm{discharge/area} \quad (12)$$

We also calculated cationic weathering rates for silicate and carbonate rocks ($Cation_{sil}$ and $Cation_{carb}$), and the calculated results for the four rivers are listed in Table 3. The SWR and cation-silicate weathering rate ($Cation_{sil}$) of Heihe, Shule, Beida, and Shiyang River is 0.81, 0.76, 2.04, and 0.93 ton km^{-2} a^{-1}, and 0.64, 0.52, 1.13, and 0.68 ton km^{-2} a^{-1}, respectively. The CWR and evaporite weathering rates of these rivers range from 1.91 to 9.23 ton km^{-2} a^{-1}, and from 1.27 to 3.84 ton km^{-2} a^{-1}, respectively.

Conclusions

Compared with the global river average, these rivers in the arid region are significantly enriched in dissolved solids. The dominance of Ca^{2+}, Mg^{2+}, and HCO_3^-, and significantly high content of SO_4^{2-} and Cl^- in major ion composition is the typical characteristics of these rivers. The intercorrelations between ion and Sr isotopic ratios suggest predominance of three end-members of rock weathering sources to the solutes in the river water, which are evaporite, carbonate, and silicate weathering. The dissolved load of the rivers is dominated by evaporite dissolution and carbonate weathering. Average proportion of the dissolved cations in river water from silicates weathering is 23.5,

10.8, 12.1, and 18.2 % for Heihe, Shule, Beida, and Shiyang River, respectively. The weathering rates of silicate and carbonate are 0.81, 0.76, 2.04, and 0.93 ton km^{-2} a^{-1}, and 1.91, 3.48, 9.23, and 2.89 ton km^{-2} a^{-1} for these rivers, respectively.

Acknowledgments This work was financially supported by the National Basic Research Program of China ("973 Program", Grant No. 2013CB956401), the "Strategic Priority Research Program" of the Chinese Academy of Sciences (Grant No. XDB03020400), Natural Science Foundation of China (Grant Nos. 41173114 and 41402323), the international postdoctoral exchange fellowship program (Grant No. 20140045) and China Postdoctoral Science Foundation Grant (2014M550833). The authors appreciate the constructive comments from three anonymous reviewers to improve the manuscript.

References

Berner RA, Lassaga AC, Garrels RM (1983) The carbonate-silicate geochemical cycle and its effect on atmospheric carbon dioxide over the past 100 million years. Am J Sci 283:641–683

Bluth GJS, Kump LR (1994) Lithological and climatological controls of river chemistry. Geochim Cosmochim Acta 58:2341–2359

Chen JS, Wang FY, Xia XH, Zhang LT (2002) Major element chemistry of the Changjiang (Yangtze River). Chem Geol 187:231–255

Chen J, Li G, Yang J, Rao W, Lu H, Balsam W, Sun Y, Ji J (2007) Nd and Sr isotopic characteristics of Chinese deserts: implications for the provenances of Asian dust. Geochim Cosmochim Acta 71:3904–3914

Chetelat B, Liu CQ, Zhao ZQ, Wang QL, Li SL, Li J, Wang BL (2008) Geochemistry of the dissolved load of the Changjiang Basin Rivers: anthropogenic impacts and chemical weathering. Geochim Cosmochim Acta 72:4254–4277

Feng YM, He SP (1996) Tectonics and Orogeny of Qilian Mountains. Geological Publishing House, Beijing, pp 1–135 **(in Chinese with English abstract)**

Gaillardet J, Dupré B, Allègre CJ, Négrel P (1997) Chemical and physical denudation in the Amazon River Basin. Chem Geol 142:141–173

Gaillardet J, Dupré B, Louvat P, Allègre CJ (1999) Global silicate weathering and CO_2 consumption rates deduced from the chemistry of large rivers. Chem Geol 159:3–30

Galy A, France-Lanord C (1999) Weathering processes in the Ganges—Brahmaputra basin and the riverine alkalinity budget. Chem Geol 159:31–60

Gao Q, Tao Z, Huang X, Nan L, Yu K, Wang Z (2009) Chemical weathering and CO_2 consumption in the Xijiang River basin, South China. Geomorphology 106:324–332

Gibbs RJ (1970) Mechanisms controlling world water chemistry. Science 170:1088–1090

Gislason SR, Arnorsson S, Armansson H (1996) Chemical weathering of basalt in southwest iceland: effects of runoff, age of rocks and vegetative/glacial cover. Am J Sci 296:837–907

Hou QY, Zhao ZD, Zhang HF, Zhang BR, Chen YL (2006) Indian Ocean-MORB type isotopic signature of Yushigou ophiolite in North Qilian Mountains and its implications. Sci China Earth Sci 49:561–572

Hu M, Stallard RF, Edmond JM (1982) Major ion chemistry of some large Chinese rivers. Nature 298:550–553

Hu F, Yang X (2016) Geochemical and geomorphological evidence for the provenance of aeolian deposits in the Badain Jaran Desert, northwestern China. Quat. Sci. Rev. 131:179–192

Huh Y, Tsoi MY, Zaitsev A, Edmond JM (1998) The fluvial geochemistry of the rivers of Eastern Siberia: I. Tributaries of the Lena River draining the sedimentary platform of the Siberian Craton. Geochim Cosmochim Acta 62:1657–1676

Jin Z, You C, Yu J, Wu L, Zhang F, Liu H (2011) Seasonal contributions of catchment weathering and eolian dust to river water chemistry, northeastern Tibetan Plateau: chemical and Sr isotopic constraints. J Geophys Res 116:327–336

Louvat P, Allégre CJ (1997) Present denudation rates at Réunion island determined by river geochemistry: basalt weathering and mass budget between chemical and mechanical erosions. Geochim Cosmochim Acta 61:3645–3669

Meybeck M (1987) Global chemical weathering of surficial rocks estimated from river dissolved loads. Am J Sci 287:401–428

Meybeck M (2003) Global occurrence of major elements in rivers. In: Drever JI (ed) Treatise on Geochemistry, Surface and Ground Water, Weathering, and Soils. Elsevier, pp 207–223

Meyer B, Tapponnier P, Bourjot L, Metivier F, Gaudemer Y, Peltzer G, Guo S, Chen Z (1998) Crustal thickening in Gansu-Qinghai, lithospheric mantle subduction, and oblique, strike-slip controlled growth of the Tibet plateau. Geophys J Int 135(1):1–47

Millot R, Gaillardet J, Dupré B, Allègre CJ (2003) Northern latitude chemical weathering rates: clues from the Mackenzie River Basin, Canada. Geochim Cosmochim Acta 67:1305–1329

Nakano T, Yokoo Y, Nishikawa M, Koyanagi H (2004) Regional Sr–Nd isotopic ratios of soil minerals in north China as Asian dust fingerprints. Atmos Environ 38:3061–3067

Négrel P, Allègre CJ, Dupré B, Lewin E (1993) Erosion sources determined by inversion of major and trace element ratios and strontium isotopic ratios in river water: the Congo Basin case. Earth Planet Sci Lett 120:59–76

Palmer MR, Edmond JM (1992) Controls over the strontium isotope composition of river water. Geochim Cosmochim Acta 56:2099–2111

Qin J, Huh Y, Edmond JM, Du G, Ran J (2005) Chemical and physical weathering in the Min Jiang, a headwater tributary of the Yangtze River. Chem Geol 227:53–69

Sarin MM, Krishnaswami S, Dilli K (1989) Major ion chemistry of the Ganga–Brahmaputra river system: weathering processes and fluxes to the Bay of Bengal. Geochim Cosmochim Acta 53:977–1009

Song SG, Zhang LF, Niu YL, Song B, Zhang GB, Wang QJ (2004) Zircon U–Pb SHRIMP ages of eclogites from the North Qilian Mountains in NW China and their tectonic implication. Chin Sci Bull 49:848–852

Stallard RF, Edmond JM (1983) Geochemistry of the Amazon: 2. Influence of geology and weathering environment on the dissolved load. J Geophys Res 88:9671–9688

Stallard RF, Edmond JM (1987) Geochemistry of the Amazon: 3. Weathering chemistry and limits to dissolved inputs. J Geophys Res 92:8293–8302

Summerfield MA, Hulton NJ (1994) Natural controls of fluvial denudation rates in major world drainage basins. J Geophys Res 99:13871–13883

Tapponnier P, Meyer B, Avouac JP, Peltzer G, Gaudemer Y, Guo S, Xiang H, Yin K, Chen Z, Cai S, Dai H (1990) Active thrusting and folding in the Qilian Shan, and decoupling between upper crust and mantle in northeastern Tibet. Earth Planet Sci Lett 97(3):382–403

Tseng CY, Yang HJ, Yang HY, Liu DY, Tsai CL, Wu HQ, Zuo GC (2007) The Dongcaohe ophiolite from the North Qilian Mountains: a fossil oceanic crust of the Paleo-Qilian Ocean. Chin Sci Bull 52:2390–2401

Viers J, Dupré B, Braun JJ, Deberdt S, Angeletti B, Ngoupayou JN, Michard A (2000) Major and trace element abundances, and strontium isotopes in the Nyong basin rivers (Cameroon):

constraints on chemical weathering processes and elements transport mechanisms in humid tropical environments. Chem Geol 169:211–241

White AF, Blum AE (1995) Effect of climate on chemical weathering in watersheds. Geochim Cosmochim Acta 59:1729–1747

Wu HQ, Feng YM, Song SG (1993) Metamorphism and deformation of blue schist belts and their tectonic implications, North Qilian Mountains, China. J Metamorph Geol 11:523–536

Wu CL, Yang JS, Yang HY, Wooden J, Shi RD, Chen SY, Zheng QG (2004) Dating of two types of granite from North Qilian, China. Acta Petrol Sin 20:425–432 **(in Chinese with English abstract)**

Wu LL, Huh Y, Qin JH, Du G, Van Der Lee S (2005) Chemical weathering in the Upper Huang He (Yellow River) draining the eastern Qinghai Plateau. Geochim Cosmochim Acta 69:5279–5294

Wu W, Xu S, Yang J, Yin H (2008) Silicate weathering and CO_2 consumption deduced from the seven Chinese rivers originating in the Qinghai-Tibetan Plateau. Chem Geol 249:307–320

Xu ZF, Liu CQ (2007) Chemical weathering in the upper reaches of Xijiang River draining the Yunnan-Guizhou Plateau, Southwest China. Chem Geol 239:83–95

Xu ZF, Liu CQ (2010) Water geochemistry of the Xijiang basin rivers, South China: chemical weathering and CO_2 consumption. Appl Geochem 25:1603–1614

Xu Z, Shi C, Tang Y, Han H (2011) Chemical and strontium isotopic compositions of the Hanjiang basin rivers in China: anthropogenic impacts and chemical weathering. Aqua Geochem 17:243–264

Yang JS, Xu ZQ, Zhang JX, Song SG, Wu CL, Shi RD, Li HB, Brunel M (2002) Early Palaeozoic North Qaidam UHP metamorphic belt on the north-eastern Tibetan Plateau and a paired subduction model. Terra Nova 14:397–404

Yokoo Y, Nakano T, Nishikawa M, Quan H (2001) The importance of Sr isotopic composition as an indicator of acid-soluble minerals in arid soils in China. Water Air Soil Poll 130:763–768

Yokoo Y, Nakano T, Nishikawa M, Quan H (2004) Mineralogical variation of Sr–Nd isotopic and elemental compositions in loess and desert and from the central Loess Plateau in China as a provenance tracer of wet and dry deposition in the northwestern Pacific. Chem Geol 204:45–62

Zhang J, Huang WW, Létolle R, Jusserand C (1995a) Major element chemistry of the Huanghe (Yellow River), China-weathering processes and chemical fluxes. J Hydrol 168:173–203

Zhang J, Takahashi K, Wushiki H, Yabuki S, Xiong JM, Masuda A (1995b) Water geochemistry of the rivers around the Taklimakan Desert (NWChina): crustal weathering and evaporation processes inarid land. Chem Geol 119:225–237

Zhang JX, Meng FC, Wan YS (2007a) A cold Early Palaeozoic subduction zone in the North Qilian Mountains, NW China: petrological and U–Pb geochronological constraints. J Metamorph Geol 25:285–304

Zhang SR, Lu XX, Higgitt DL, Chen CTA, Sun HG, Han JT (2007b) Water chemistry of the Zhujiang (Pearl River): natural processes and anthropogenic influences. J Geophys Res 112:137–161